Integrated Planar Antennas at Terahertz Waves

A. Semenov, H. Richter, B. Günther, H.-W. Hübers, J. Karamarkovic

***Abstract* — We present the terahertz performance of integrated lens antennas consisting of a double-slot or a log-spiral planar feed and a synthesized elliptical lens. The radiation pattern and the impedance of the planar feeds are computed using the method of moments; the collimating action of the lens is modeled using the physical-optics approach based on the Huygens principle. In the frequency range from 1.5 to 3 THz (double-slot feed) and 0.6 to 5 THz (log-spiral feed) the measured antenna efficiency and radiation pattern correspond fairly well with the results of simulations approving this simulation technique as a reliable tool for the antenna design.**

***Index Terms*—planar antennas, impedance, beam pattern**

I. Introduction

Exploring the terahertz frequency range becomes an important trend in planetary science, astronomy and security research. For terahertz receivers the planar integrated quasioptical technology is expected to be a preferable alternative to wave-guide based front ends. Although corrugated horns can be fabricated for frequencies up to 2.5 THz, they are getting more expensive to manufacture and the effect of misalignments becomes more severe when the frequency increases. Recent progress in nano-structuring and micro-machining allows reliably producing and aligning planar antenna structures on dielectric surfaces with an accuracy sufficient for the terahertz range. Log-periodic, log-spiral, double-slot and double-dipole feed antennas integrated with quartz or silicon lenses have been shown to successfully couple radiation in the frequency range from 30 GHz to 5.2 THz. However, designing an integrated quasioptical front-end requires reliable modeling of the feed-antenna performance. A semi-analytical, lumped element technique that was implemented so far provides results inconsistent with the experimental data at frequencies above a few terahertz [1]. The main reason, e.g. for a double-slot feed, is that this technique neglects frequency-dependent parasitic impedances appearing at the points where virtual lumped elements are connected to each other. As a result, experimentally verified resonance frequencies of the double-slot feeds do not coincide with the computed resonance frequencies. Although the discrepancy can be partly relaxed taking into account the geometric inductance of the detector used for experimental evaluation, the remaining inconsistence is rather large. This obstacles the feed design and engineering of the entire integrated antenna.

In this work we have applied the method of moments (MoM) to the entire feed structure including the slots as well as imbedding and interconnecting elements. The MoM solution was then used as an input for the physical-optics ray-tracing (PORT) procedure to obtain the beam parameters of the integrated lens antenna. The performance of integrated antennas was experimentally evaluated in combination with a hot-electron bolometer. We compare simulated and measured performance of integrated antennas with double-slot planar feeds and complementary log-periodic planar feeds and verify this technique at frequencies from 1.5 THz to 3 THz and from 0.6 to 5.2 THz, respectively.

II. Simulation Procedure

A. Feed antennas

The full wave method of moments reveals the current and charge density distribution in the antenna by solving numerically Maxwell equations with boundary conditions on a virtual mesh superimposed on the real structure. The fields at an arbitrary observation point can be computed via scalar and vector potentials generated by the source densities. We used the FEKO software package [2] that combines the accurate method of moments with the physical optics approach and the uniform theory of diffraction to obtain fields radiated by our planar feeds. We applied this technique to the double-slot and log-periodic planar feeds printed on the plane boundary of a dielectric. The geometry of the feeds used in this study is defined in Fig. 1, 2, the sizes of the feeds are shown in Table I

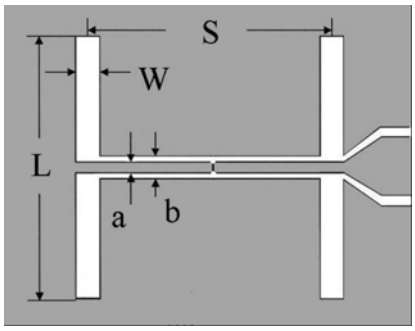

Fig. 1. Layout of a double-slot feed antenna. Gray color denotes the gold layer, white color – the dielectric. The bolometer (or the excitation slit) is located in the middle of the co-planar line connecting vertical slots.

A. Semenov, H. Richter, B. Günther and H.-W. Hübers are with the DLR institute of Planetary Research, 12489 Berlin, Germany. (corresponding author e-mail: Alexei.Semenov@dlr.de)

J. Karamarkovic is with the Faculty of Civil Engineering and Architecture, University of Nis, Serbia and Montenegro, fizika@gaf.ni.ac.yu

TABLE I
SIZES OF THE STUDIED DOUBLE-SLOT FEEDS.

Feed	a, μm	b, μm	L, μm	S, μm	W, μm
TWS1	2	4	60	32	4
TWS2	2.2	3.3	40	21	2.2
TWS3	2	4	33.5	20	2.4
TWS4	2.2	3.3	46	24	3
TWS5	3.6	2.4	30	17	2.4
TWS6	2	4	50	28	3.6
TWS7	3.6	5.1	55	30	3
TWS8	2	4	46	28	3

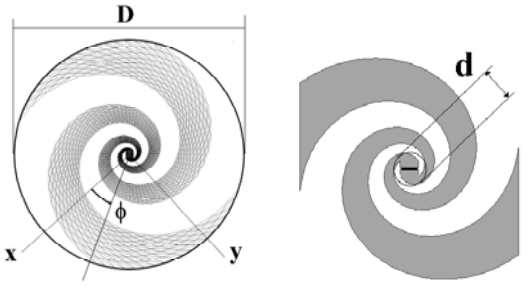

Fig. 2. Left: Full structure of the spiral feed and the mesh used for the MoM simulation. The angular position of the beam-cut is defined by the azimuth angle ϕ. Right: The smallest size *d* of the feed and the excitation slit. The parameter a = 0.36 [3] was chosen to build the arms of the feed antenna according to $R = R_0 \exp(a\,\phi)$ with ϕ been the angle and *R* the distance from the geometric center of the feed.

TABLE II
SIZES OF THE STUDIED LOG-SPIRAL FEEDS.

Feed	D, μm	d, μm
DLR_a	48	2.25
DLR_c	130	11.2

and Table II. MoM simulations were made for feeds on Si half-space cut out from a 70-nm thick gold layer.

B. Current Distribution

Double Slot: For simulations we chose the squared gold sheet with a size of 100 x 100 μm^2 that contained a double-slot feed positioned in the center of the square. We applied a uniform voltage excitation along the infinitesimally thin slit cut in the middle of the co-planar waveguide across its central line. Fig. 3 (left) shows the distribution of high-frequency 2.5 THz current in the TWS2 feed as resulted from MoM simulation. An excess current appears around the connections between the co-planar waveguide and slots. This contradicts to the lumped-element semi-analytical model, which suggests the smallest current density near the central part of each slot. The excess current modifies the feed impedance that changes the resonance frequency of the antenna.

Log-spiral: We applied a uniform excitation along the infinitely thin slit in the geometric center of the feed (Fig. 2, right panel). The overall size of a log-spiral feed is defined by the outer and the inner diameter. The outer diameter (*D*) is the diameter of the smallest circle that encompasses the feed structure. The inner diameter (*d*) is the smallest diameter where the arms still obey the spiral equation. Connecting terminals are formed inside the circle having the diameter *d*.

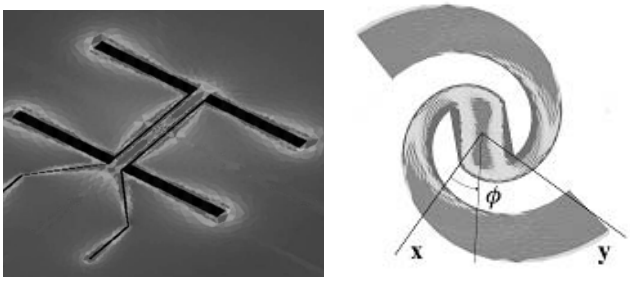

Fig. 3. Left: Distribution of the high-frequency current in the feed TWS2 obtained with MoM. Black denotes the dielectric. Right: Distribution of the high-frequency current in the spiral feed.

The electric current distribution in the central part of the DLR_c feed obtained by the MoM is shown in Fig. 3 (right panel). As it was expected, due to the skin effect [4] the high-frequency current flows mostly along the edges of the feed structure.

C. Antenna Impedance

Double Slot: The simulated impedance for the feed TWS2 is shown in Fig. 4 (upper panel). The frequency dependence of the real and imaginary parts of the feed impedance seen from the excitation slit has a certain similarity to the frequency dependence of the impedance computed for two slots without connecting co-planar waveguide [5]. However, changes introduced by the co-planar waveguide are clearly visible. The radiation coupling efficiency of the feed antenna reaches the maximum value when the imaginary component of the impedance becomes zero. For TWS2 feed corresponding resonance frequency appears approximately between 2.2 THz and 2.5 THz. In the receiving mode, the frequency resulting in the best coupling additionally depends on the impedance of the detector connected to the feed.

Log-Spiral: The simulated antenna impedance is shown in Fig. 4 (lower panel). In the whole frequency range of simulation the impedance of our feed antennas has a non-negligible imaginary component. That contradicts to the simple theory suggesting a real impedance for a free-standing complementary planar antenna. For the DLR_c feed in the frequency range up to 2.5 THz, the real part of the impedance remains almost constant and exceeds noticeably the imaginary component. Thus this antenna may be qualified as frequency-independent only in the frequency interval from 1 THz to 2.5 THz.

D. Bolometer Impedance

In order to compare the measured and simulated performance of our antennas we also modeled the impedance

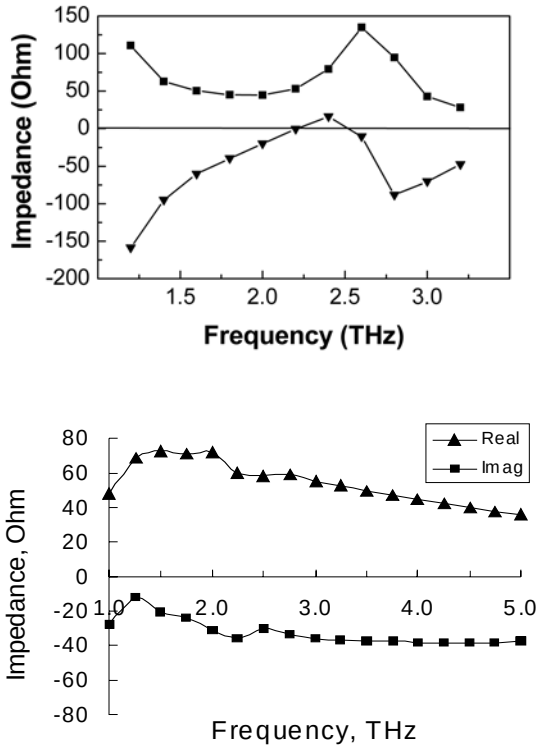

Fig. 4. Upper panel: Real (squares) and imaginary (triangles) components of the impedance computed for the TWS2 feed. Lower panel: Impedance of a log-spiral feed DLR_c. Lines are guides for the eye.

of the hot-electron bolometer, which was used for the experimental evaluation. Assuming a frequency independent conversion efficiency of the bolometer and taking into account the skin effect in the bolometer itself [5], we derived the complex HEB impedance Z_B. This results in the following antenna gain G

$$G = \frac{4Z_{B1}(Z_1 + Z_K) + Z_{B2}Z_2}{(Z_1 + Z_{B1} + Z_K)^2 + (Z_2 + Z_{B2})^2} M \qquad (1)$$

$$Z_B = R_n \frac{w(1+j)}{4\delta} \coth\left[\frac{w(1+j)}{4\delta}\right] = Z_{B1} + jZ_{B2}$$

where $Z_A = Z_1 + j\,Z_2$ is the impedance of the feed, R_n is the normal dc resistance of the bolometer, Z_K is the contact resistance and $\delta = (2\mu_0\omega/\rho)^{1/2}$ and ρ are the skin depth and the normal-state resistivity of the bolometer, respectively. The factor M accounts for coupling losses, which have been estimated using attenuation of optical elements [4]. Fig. 5 shows the impedance computed according Eq. 1 for a 2-μm wide bolometer. Even for a relatively small HEB, the imaginary part of the impedance compares with the real part at frequencies above 1 THz. Since the contact resistance for a particular specimen is not well known, for gain simulations we used $Z_K = 0.4\ R_n$. For the integrated antenna including planar feed and HEB, maximum power is delivered to the HEB in case of the conjugate matching: $Z_{B2} = -Z_2$.

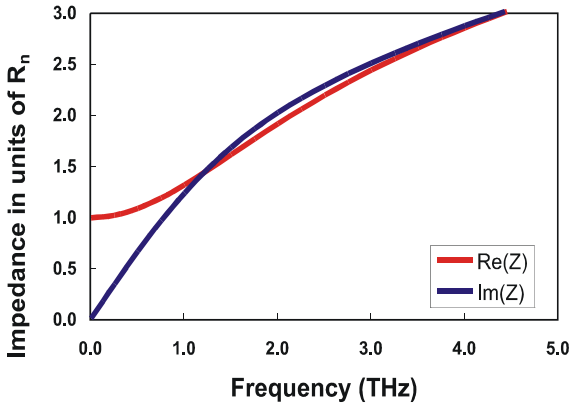

Fig. 5. Calculated impedance of the 2-μm wide HEB.

E. Ray-Tracing

Given the Rayleigh distance less than one millimeter, the surface of a lens with a diameter of few millimeter appears in the far-field regime of the feed. Therefore, as an input for the PORT procedure we used the far-field results delivered by the MoM simulations. The electric and magnetic fields at the surface inside the lens were decomposed into the s- and p-components. Then each component was multiplied with an appropriate Fresnel transmission coefficient and the resulting components were combined again to obtain the electric E and magnetic H fields just outside the lens. Equivalent electric and magnetic sources outside the lens were defined [6] as

$$\vec{J}_S = \vec{n}1 \times \vec{H} \quad and \quad \vec{M}_S = -\vec{n}1 \times \vec{E} \qquad (2)$$

where $\boldsymbol{n1}$ is the unit vector normal to the lens surface. The electric field at the observation point at a distance r from the running point on the surface, $\boldsymbol{e}_r$ being the unit vector of this distance, was obtained by integrating over the lens surface A

$$\vec{E} = \frac{j\,k_0}{4\pi\,\omega\,\varepsilon_0} \times \qquad (3)$$

$$\iint_S \left[\vec{J}_S - \left(\vec{J}_S \cdot \vec{e}_r\right)\vec{e}_r + \frac{1}{Z_0}\left(\vec{M}_S \times \vec{e}_r\right)\right] \frac{e^{-j\,k_0 r}}{r}\, dA$$

with k_0, Z_0 and ω been the free-space wave-vector, the impedance of free space and the angular frequency, respectively. We computed the beam profile formed by an extended hemi-spherical lens (radius $R_L = 6$ mm, index of refraction $n = 3.42$) with different extension lengths ε.

Results for the TWS6 feed at 1.9 THz are shown in Fig. 6. The –3 dB width of the main lobe reaches the minimum of 1.55° for $\varepsilon = 2.4$ mm while the side-lobes drop to the lowest level at $\varepsilon = 2.5$. An acceptable level (-14 dB) of side lobes and an almost Gaussian shape of the main lobe are both achieved for an intermediate extension length of 2.45 mm that brings

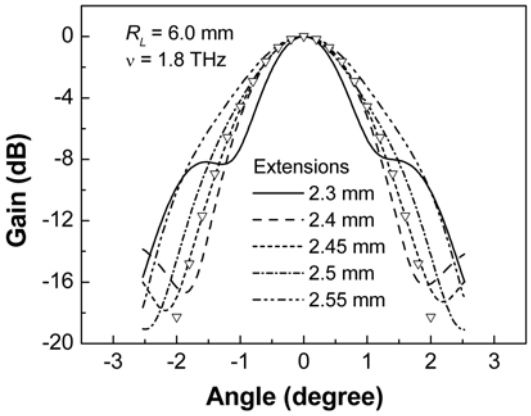

Fig. 6. Computed by E-plane 1.8-THz beam profile of the TWS6 feed integrated with a 6 mm radius lens with different extension lengths. Triangles show an analytical Gaussian profil.

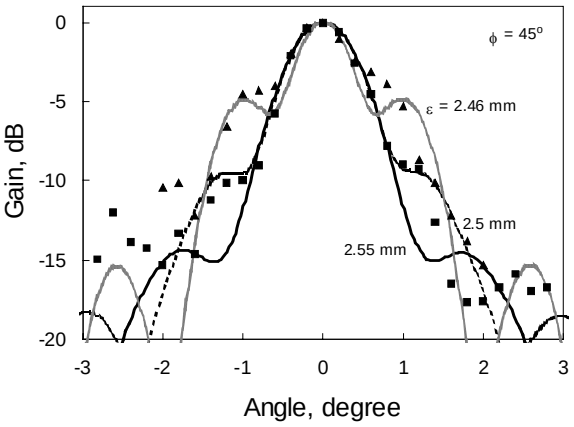

Fig. 8. Radiation pattern of integrated lens antennas with the DLR_a feed at 2.5 THz. Experimental data are shown by squares for scans at ϕ = 45° and by triangles for scans at ϕ = 135°. The lines present the result of MoM + PO ray-tracing simulations. Extension lengths are marked at the curves.

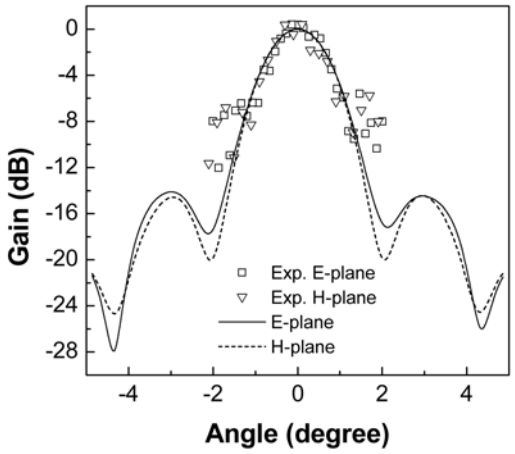

Fig. 7. Simulated (lines) and experimentally measured (squares and triangles) beam pattern of the integrated antenna with the TWS6 feed at 1.9 THz. The extension length in both cases was 2.45 mm.

the feed to the most distant focal point $\varepsilon = R_L/(n\text{-}1)$ of a corresponding synthesized elliptical lens [7]. At this optimal extension length the simulated beam profile of the integrated antenna is practically the same in both E- and H-planes down to –15 dB level (Fig. 6). However, an accuracy of the feed positioning better than 100 μm is required in order to keep side-lobes below -10 dB.

III. Experiment

We evaluated experimentally the performance of integrated lens antennas in the receiving mode. Hot-electron bolometers were incorporated in the planar feed and operated as either heterodyne or integrating direct detector. The feed was printed on a 350 μm thick Si substrate from a 70 nm thick gold film. HEBs were fabricated from a superconducting NbN film with a nominal thickness of about 4 nm and a sheet resistance of ≈ 600 Ohm just above the superconducting transition. Fabrication details are presented elsewhere [4]. A typical bolometer had an area of one tenth of a square, i.e. the width W = 1.8 μm amounted at ten times the length, and the corresponding normal-state resistance R_n = 60±6 Ohm as determined by the accuracy of the manufacturing process. The substrate carrying the feed with the bolometer was glued with its back-side onto the flat optically polished side of an extended hemispherical silicon lens. The lens had a radius of 6 mm. A 2.1-mm extension of the lens together with the substrate thickness positioned the feed in the more distant elliptical focus. The lens with the HEB was mounted in a dewar with optical access through a wedged TPX vacuum window and a cold (77 K) quartz filter.

In the heterodyne regime, the intermediate frequency signal was amplified and registered within a bandwidth of 75 MHz centered at 1.5 GHz. An optically pumped FIR gas laser providing lines at frequencies 0.69, 1.63, 2.53, 3.1, 4.3 and 5.2 THz was used as a local oscillator (LO). Signal radiation and LO radiation were superimposed by a 6 μm thick Mylar beam splitter. The double sideband (DSB) noise temperature of the receiver was measured by the Y-factor method. Hot and cold loads (Eccosorb) at 293 K and 77 K alternatively covered the antenna beam. The beam pattern of the integrated antenna was measured with a small 5-mm high-pressure mercury lamp moving in the far field of the integrated antenna. The output heterodyne signal was recorded as a function of the lamp position.

Fast-Fourier-Transform (FTS) measurements were performed with the mixer kept at the middle of the superconducting transition and operated in the direct detection regime. We used an interferometer with a 12-mm thick Mylar beam splitter and a mercury discharge lamp as radiation

source.

A. Experimental Data versus Simulation

Double-Slot: The measured beam pattern of the integrated lens antenna with the TWS6 feed at 1.9 THz is shown in Fig. 7 along with the computed beam profiles. Due to the large distance betwen the lamp and the antenna, the nose was relatively high not allowing us to reach side-lobe level. However, an overall width of the mail lobe corresponds fairy well with the results of simulation.

Log-spiral: Experimentally measured radiation pattern of integrated lens antennas with the DLR_a feed at 2.5 THz is shown in Fig. 8 along with the computed beam profiles. The sensitivity at 2.5 THz was relatively low resulting in a high noise level that did not allow us to clearly distinguish side-lobes. Another reason is that the 0.3° angular size of our hot-source was comparable to the angular spacing of the side lobes. However, the shape of the measured radiation pattern agrees with the results of simulations.

B. Comparison with FTS spectra

For all studied feeds, we have found a reasonably good agreement between measured FTS spectrum, system noise temperatures and simulated frequency dependence of the antenna gain.

Double slot: Data for three selected feeds are presented in Fig. 9 (upper panel). Measured noise temperatures correlate better with simulated gain spectra than with FTS spectra, which are systematically shifted to lower frequencies. We speculate, that this shift may be due to the difference between the HEB impedance in the heterodyne and the direct detection mode. Another outcome of our study also noticed in Ref. 1 is that commonly used design rules [9] to achieve the resonance wavelength λ_0, i.e. $L \approx 0.33\ \lambda_0$, $S = 0.17\ \lambda_0$ and $W = 0.05\ \lambda_0$, practically result in a double-slot feed with a somewhat larger resonance wavelength. The difference gradually grows with the operation frequency.

Log-spiral: The lower panel of Fig. 9 compares the simulated gain and the reciprocal noise temperature for integrated antennas with two different log-spiral feeds. There is a good match through the whole frequency range besides the lowest frequency where the device performs better than the simulation predicts. We suggest that the actual conversion efficiency of a HEB increases at frequencies smaller than the frequency corresponding to the energy gap of NbN.

IV. Conclusion

In conclusion, we have demonstrated that the full method of moments applied to the entire feed structure and combined with the physical-optics ray-tracing technique adequately models both the radiation coupling abilities and the beam pattern of an integrated lens antenna at terahertz frequencies. The approach can be used as an engineering tool for the design of quasioptical front-ends in the state-of-the-art heterodyne receivers.

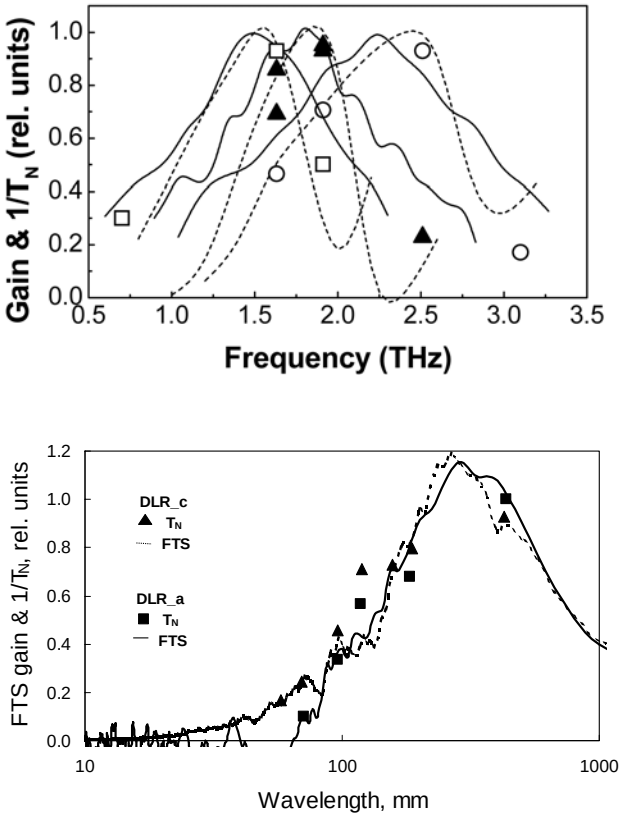

Fig. 9. Upper panel: Simulated gain versus frequency for the double-slot feeds (dotted lines), experimentally measured FTS spectra (solid lines) and reciprocal noise temperature of integrated antennas with (from left to right) TWS1 (squares), TWS6 (triangles) and TWS2 (circles) feeds. Lower panel: FTS spectra and reciprocal noise temperatures of integrated antennas with log-spiral feeds.

References

[1] R.A. Wyss, A. Neto, W.R. McGrath, B. Bumble, H. LeDuc, in Proceedings of the 11th Int. Symposium on Space Terahertz Technology, Uni. of Michigan, Ann Arbor, MI, pp. 388-397, May 2000.

[2] FEKO: a computer code for the analysis of electromagnetic problems, http://www.feko.info/.

[3] Yu. P. Gousev, A. D. Semenov, E. V. Pechen, A. V. Varlashkin, R. S. Nebosis, and K. F. Renk, "Broadband coupling of terahertz radiation to an YbaCuO hot-electron bolometer mixer," Supercond. Sci. Technol. Vol. 9, pp. 779-787, 1996.

[4] A. D. Semenov, H.-W. Hübers, J. Schubert, G. N. Gol'tsman, A. I. Elantiev, B. M. Voronov, and E. M. Gershenzon, "Design and Performance of the Lattice Cooled Hot-Electron Terahertz Mixer," Journal of Applied Physics, vol. 88, pp. 6758-6766, December 2000.

[5] M. Kominami, D.M. Pozar and D.H. Schaubert, *IEEE Transactions on Antennas and Propagations* **33**, 600 (1985).

[6] J.A. Balanis, *Antenna Theory: Analysis and Design*, John Wiley & Sons, Inc., pp. 448-450, 1982.

[7] D.F. Fillipovic, S.S. Gearhart, G.M. Rebeiz, *IEEE Transactions on Microwave Theory and Techniques* **41**, 1738 (1993).

[8] M. Bin, M.C. Gaidis, J. Zmuidzinas, T.G. Philips, H.G. LeDuc, *Appl. Phys. Lett.* **68**, 1714 (1996).